Surface & Coatings Technology 309 (2017) 795–804

Contents lists available at ScienceDirect

Surface & Coatings Technology

journal homepage: www.elsevier.com/locate/surfcoat

Fabrication of superhydrophobic iron with anti-corrosion property by ultrasound

Toktam Rezayi [a], Mohammad H. Entezari [a,b,*]

[a] Sonochemical Research Center, Department of Chemistry, Ferdowsi University of Mashhad, 91779 Mashhad, Iran
[b] Environmental Chemistry Research Center, Department of Chemistry, Ferdowsi University of Mashhad, 91779 Mashhad, Iran

ARTICLE INFO

Article history:
Received 14 June 2016
Revised 27 October 2016
Accepted in revised form 28 October 2016
Available online 29 October 2016

Keywords:
Superhydrophobic surface
Iron substrate
Stearic acid
Ultrasound

ABSTRACT

The creation of superhydrophobic (SH) surfaces requires a combination of surface roughness and surface free energy reduction. For this purpose, wire-like ZnO particle (with micro scale in length and nano-scale in width) deposition was performed on iron surface by means of an ultrasound approach. After that, stearic acid (STA) ethanol solution was utilized for surface energy reduction. The optimization of various parameters was conducted based on Minitab software and Taguchi design method. After reaching a SH iron with ultrasound at optimized conditions, the corrosion resistance was compared between SH iron resulted by classical method (SH iron (C)) under the same conditions as ultrasound method (SH iron (U)). The potentiodynamic estimates indicated that when ultrasound was employed for particle deposition, the corrosion current (I_c) was 1000 times lower than that for bare iron one. However, using classical method for particle deposition had no dramatic effect on corrosion resistance. Moreover, when ultrasound was used for particle deposition, the stability of the resulted SH iron versus immersion in NaCl solution (3.5%) was higher compared to SH iron acquired by classical technique. Finally, different characterization methods were used for further study. For example, scanning electron micrograph (SEM) was carried out for topographical investigation of the surfaces obtained. Other techniques such as attenuated total reflection in combination with Fourier transform infrared (ATR-FTIR) and energy-dispersive X-ray spectroscopy (EDX) verified ZnO particle deposition. Moreover, for verification of STA grafting on SH iron, EDX analysis was helpful.

1. Introduction

One of the significant properties related to the solid surfaces is wettability that is controlled using both surface morphology and chemical composition of surfaces. SH surfaces with water contact angle (WCA) larger than 150°, have appealed greatly interest in central research and prospective industrial applications [1–3]. These surfaces are classified into two categories based on sliding angle (SA) value. These classes are named as low-adhesive and high-adhesive SH surfaces. Low–adhesive SH surfaces possess SA value lower than 10°. In this case, water droplet can roll easily as SH surface tilted partially. In contrast, high-adhesive SH surfaces have high SA value. In this instance, water droplets stick to the surface even with turning upside down the surface.

The lotus leaves, the rice leaves and the legs of water strider are examples of low-adhesive SH surfaces in natural world. Moreover, the usual high-adhesive SH surfaces in natural surroundings are rose petals, peanut leaves, and feet of bees. Because of numerous applications of low-adhesive SH surfaces, great studies has been focused on these surfaces [4,5]. The new researches exhibit that the superhydrophobicity of the lotus leaves mainly results from the existence of dualistic structures at micro and nano-meter measures and waxy materials with low surface energy on the surfaces [6]. To date, several techniques such as lithography, laser etching, plasma treatment and template duplication have been established to manufacture SH surfaces based on lotus leaf structure [7–12]. The metal surfaces are simply wetted and covered with a coating of water film, causing in severe troubles counting icing and corrosion. Consequently, the design of metal products with superhydrophobicity property is sensible [13,14]. There are several works related to this issue. For example, Wei et al. [15] employed a trouble-free way to produce SH magnesium alloy. Their method consisted of etching of magnesium in copper chloride and modification of resulted surface with STA as surface free energy reducer agent. Polarization and impedance examinations demonstrated corrosion resistance enhancing of SH magnesium in comparison with bare alloy. Moreover, the SH surface exhibited long-term stability in NaCl aqueous solution (3.5%) [15].

In another work, Zhang et al. synthesized anti-corrosion magnesium alloy with SH characteristic. The superhydrophobicity was obtained using simple immersion process and modification in STA during a

* Corresponding author at: Sonochemical Research Center, Environmental Chemistry Research Center, Department of Chemistry, Ferdowsi University of Mashhad, 91779 Mashhad, Iran.
E-mail addresses: entezari@um.ac.ir, moh_entezari@yahoo.com (M.H. Entezari).

http://dx.doi.org/10.1016/j.surfcoat.2016.10.083
0257-8972/

hydrothermal production method [16]. With the exception of magnesium alloy, there are similar efforts for iron surfaces. For example, micro/nano structures were fabricated on iron surfaces via chemical etching with a solution of hydrochloric acid or galvanic substitution using silver nitrate. The modification of obtained hierarchical iron with STA led to SH iron surface. The anti-icing property examination revealed that SH iron exhibited outstanding anti-icing characteristic in comparison with bare ones [17]. In another study, Hao-Jie Song et al. used a straightforward and economic hydrothermal method based on K_2CO_3 mediated process to manufacture structures with micro/nano scales on iron plates. The vinyl triethoxysilane was employed as surface energy reducer to yield superhydrophobic property [18]. In spite of simplicity and cost-effectively of mentioned works, anti-corrosion property was not explored. However, in a study performed by Wang et al. anti-icing, UV-durability and corrosion resistance characteristics of resulted SH steel was investigated [19]. But, the surface energy reduction was carried out using 1H,1H,2H,2H-perfluorodecyltriethoxysilane (FAS-17), that is not environmentally suitable. In current study, STA as biocompatible modifier is utilized for surface energy reduction. Besides, ultrasonic waves have been employed as novel technique for ZnO particle deposition on iron substrates. Ultrasound is a competent and powerful method for the production of many materials with variable characteristics. There are several published papers related to ultrasound-assisted synthesis of different nanoparticles. For example, ZnO nanoparticles with dissimilar morphologies, Fe_3O_4 nanoparticles, gold and silver nanostructures were synthesized using ultrasound [20–23]. In spite of numerous attempts for the nanoparticle synthesis, there are a few work about utilizing ultrasound as a practical technique for particle deposition in SH creation field. Therefore, the major novelty of our work is achievement to SH iron with enhanced anti-corrosion property using ultrasound. Ultrasound generates exceptional conditions that result in special changes. These changes are due to cavitation phenomenon that is consisted of creation, expansion and collapse of bubbles in aqueous environment. The bubble collapse in heterogeneous surrounding is non-symmetric. As a result, the topography of surface can be influenced by shock waves and micro-jets creation. It is predictable that distinctive morphology has remarkable influence on the wettability of surface and durability of the acquired SH surface. In this work, ultrasound demonstrated a vital function in particle deposition to conclude SH iron surface with outstanding anti-corrosion property in corrosive environment. Moreover, in this work the ultrasound parameters have been optimized simultaneously to have higher WCA and lower SA on SH surfaces. At the end, a comparison has been conducted between anti-corrosion property of SH iron surfaces fabricated using simple immersion (classic), and ultrasound methods.

2. Experimental section

2.1. Materials

Pure Iron plate in dimensions of 20 mm × 15 mm × 1 mm was used in current work. Hexamethylenetetramine (HMT, 99%) was supplied by Samchun Company. Zinc sulfate heptahydrate ($ZnSO_4 \cdot 7H_2O$, 99%) was made available by Merck Company. Stearic acid (STA, 99%) and ethanol (96%) were purchased from BDH and Riedel companies, respectively. All chemicals were utilized as received.

2.2. Superhydrophobic iron formation with ultrasound

Firstly, the iron surfaces were polished mechanically using sand paper (400 and 800#). Afterward, the plates were washed thoroughly with distilled water, ethanol and acetone and dried at 80 °C. Then, the cleaned iron plates were vertically immersed into 50 cm^3 aqueous solution of HMT (with changeable concentration) and after 1 min sonication, 25 cm^3 aqueous solution of $ZnSO_4$ (with variable concentration) was added. Sonication was continued for various interval times at different temperatures. Schematic 1a demonstrates the experiment conducted under ultrasound. The output frequency and power of ultrasound equipment (XL 2020(were 20 Hz and 550 W, respectively. The horn tip was immersed 1 cm into the solution and located in the middle of the cell. It should be noted that calorimetry method was used for acoustic power determination for three levels of acoustic amplitude (25%, 35% and 45%). Based on this method, the acoustic power for acoustic amplitude of 25%, 35% and 45% were 0.50 W, 2.07 W and 11.33 W, respectively. The acoustic power measurements were carried out for 75 mL of solution, since the final solution volume reached to this value.

Three levels of concentrations (0.01 M, 0.05 M and 0.10 M) were selected for starting materials of HMT and $ZnSO_4$ in final solution. It is worthy to note that, for all experiment runs, the starting material molar ratio is 1:1. After withdrawing the plate from HMT-$ZnSO_4$ solution, the iron plates were rinsed completely with distilled water and dried for 1 h at 100 °C. In this stage ZnO-deposited iron surface was concluded. The surface energy reduction as a final step was performed using immersion of ZnO-deposited iron surface in STA ethanol solution with changeable concentrations and various immersion times. After moving back from STA solution, iron plates were completely rinsed with ethanol and dried for 10 min at 80 °C. It should be pointed out that the WCA and SA measurements have been accomplished on the samples after attainment to room temperature. The optimization of variables in these experiments (concentration of starting materials, reaction time, reaction temperature, acoustic amplitude, STA concentration, immersion time in STA) was carried out simultaneously with Minitab 14 software with Taguchi design method. Taguchi technique employs standard Orthogonal Arrays (OA) for creating an experiment matrix. Utilizing an OA to experiment design facilitates the study of

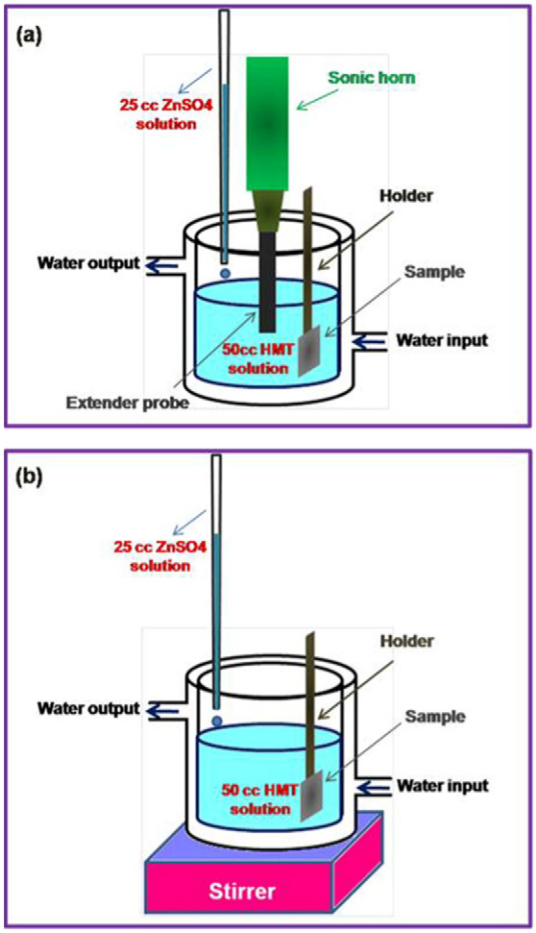

Schematic 1. a) ultrasound and b) classical deposition methods.

Table 1
Experiment design using Minitab software.

Run number	Reaction time (min)	Reaction temperature (°C)	Acoustic amplitude (%)	Starting material concentration (M)	Time immersion in STA (min)	STA concentration (g/5 cm^3 ethanol)	WCA (degree)	SA (degree)	RPD
1	5	25	25	0.01	2	0.005	41.00	90.00	1025.00
2	5	25	25	0.01	20	0.010	59.09	90.00	1025.00
3	5	25	25	0.01	60	0.025	159.89	90.00	1025.00
4	5	40	35	0.05	2	0.005	51.24	90.00	1025.00
5	5	40	35	0.05	20	0.010	133.33	90.00	1025.00
6	5	40	35	0.05	60	0.025	158.00	9.00	12.50
7	5	60	45	0.10	2	0.005	28.94	90.00	1025.00
8	5	60	45	0.10	20	0.010	121.12	90.00	1025.00
9	5	60	45	0.10	60	0.025	154.51	90.00	1025.00
10	15	25	35	0.10	2	0.010	30.00	90.00	1025.00
11	15	25	35	0.10	20	0.025	161.02	15.60	95.00
12	15	25	35	0.10	60	0.005	117.83	90.00	1025.00
13	15	40	45	0.01	2	0.010	60.16	90.00	1025.00
14	15	40	45	0.01	20	0.025	146.62	15.00	87.50
15	15	40	45	0.01	60	0.005	88.66	90.00	1025.00
16	15	60	25	0.05	2	0.010	88.33	90.00	1025.00
17	15	60	25	0.05	20	0.025	110.00	90.00	1025.00
18	15	60	25	0.05	60	0.005	145.33	90.00	1025.00
19	30	25	45	0.05	2	0.025	68.33	90.00	1025.00
20	30	25	45	0.05	20	0.005	129.00	90.00	1025.00
21	30	25	45	0.05	60	0.010	144.87	90.00	1025.00
22	30	40	25	0.10	2	0.025	36.00	90.00	1025.00
23	30	40	25	0.10	20	0.005	110.00	90.00	1025.00
24	30	40	25	0.10	60	0.010	108.00	90.00	1025.00
25	30	60	35	0.01	2	0.025	108.31	90.00	1025.00
26	30	60	35	0.01	20	0.005	124.33	90.00	1025.00
27	30	60	35	0.01	60	0.010	160.05	8.00	0.00

the influence of several controllable variables on the middling of quality characteristics. In this work, six factors, each at three levels are chosen to design of experiments based on Taguchi technique.

2.3. Superhydrophobic iron formation with simple immersion method

A simple immersion method was utilized for particle deposition to have a comparison between superhydrophobic surfaces that are resulted with both ultrasound and classic approaches. For this purpose, the pretreatment process was done as described in previous section. Then, the cleaned iron surface was immersed into HMT solution and stirred (500 rpm) for 1 min and then $ZnSO_4$ solution was added. For having a better comparison, this experiment was carried out under the optimized conditions of ultrasound method. The surface energy reduction was performed with STA ethanol solution at optimized concentration and immersion time.

2.4. Sample characterization

An attenuated total reflection in conjunction with Fourier-transform infrared spectrophotometry (ATR-FTIR, Shimadzu-IR-460 spectrometer) and energy-dispersive X-ray spectroscopy (EDX, INCA 7353, England) were utilized for chemical composition illustration of samples. In ATR-FTIR technique, the sample was kept in contact with ZnSe crystal and incident angle of IR rays was 45°. The light, which was totally reflected by the interface between the crystal and sample, was measured to attain an infrared pattern. The surface morphology was explained via a scanning electron microscope (SEM, LEO 1450 VP, Germany). A versatile technique for roughness investigation was Atomic force

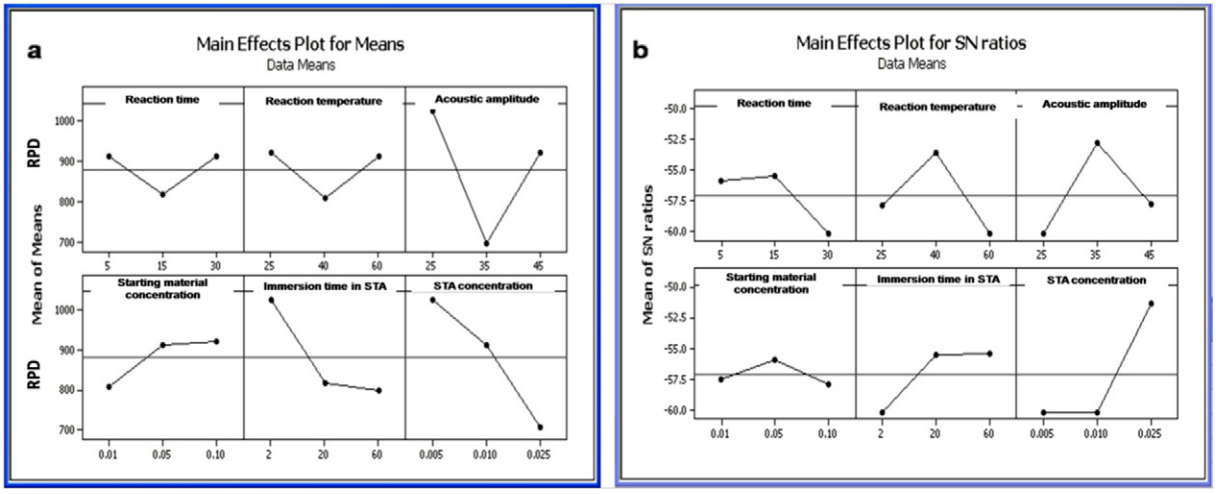

Fig. 1. a) mean of means and b) mean of SN ratios graphs.

Table 2
Optimized parameters based on Taguchi design method.

Reaction parameter	Optimized value
Reaction time	15 min
Reaction temperature	40 °C
Acoustic amplitude	35%
STA concentration	0.025 g/5 cm^3 ethanol
Immersion time in STA	60 min

microscopy (AFM, 0101/A, Iran). The images were taken under ambient temperature using nanoprobe cantilever in non-contact mode.

2.5. WCA and SA measurement

Homemade equipment was utilized For WCA calculation. 10 μL distilled water was carefully dropped by a micro syringe on iron plates. The images of droplet were captured by means of a camera (Canon SX200, Japan) and assessed with MATLAB software to WCA achievement. For SA measurement, a simple device was designed. The homemade equipment contained a mutable plane for tilting iron plate until water droplet initiated to roll off. Since, the highest situation for the movable plane was 90°, the maximum reported SA was 90°.

2.6. Electrochemical measurements

In these series of experiments, the working cell was a standard three-electrode cells. In this cell, the working electrode was iron sample with area of 1 cm^2. Moreover, the reference and counter electrodes were Na Ag/AgCl and Pt, respectively. All tests were conducted at ambient temperature (25 °C) in 3.5% NaCl aqueous solution. The scan rate of potential was 10 mV s^{-1} and potential was scanned in vicinity of OCP (open circuit potential).

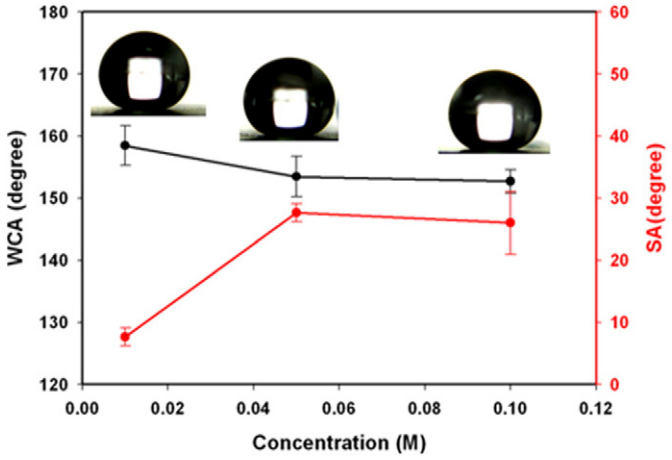

Fig. 3. WCA and SA versus starting material concentration.

3. Results and discussion

3.1. Experiment design

As it was described in experimental section, Minitab software has been utilized for optimization of different parameters. According to Taguchi technique, the L_{27}-OA runs were created (Table 1). The designed experiments were performed according to L_{27}-OA. For each experiment, the WCA and SA values were measured. Since, our purpose was to achieve a low adhesive SH characteristic; SA values were regarded as array response.

According to Taguchi design method, 27 runs of experiment were conducted. WCA and SA were measured on 27 iron surfaces in three different points of each sample and the average values were reported.

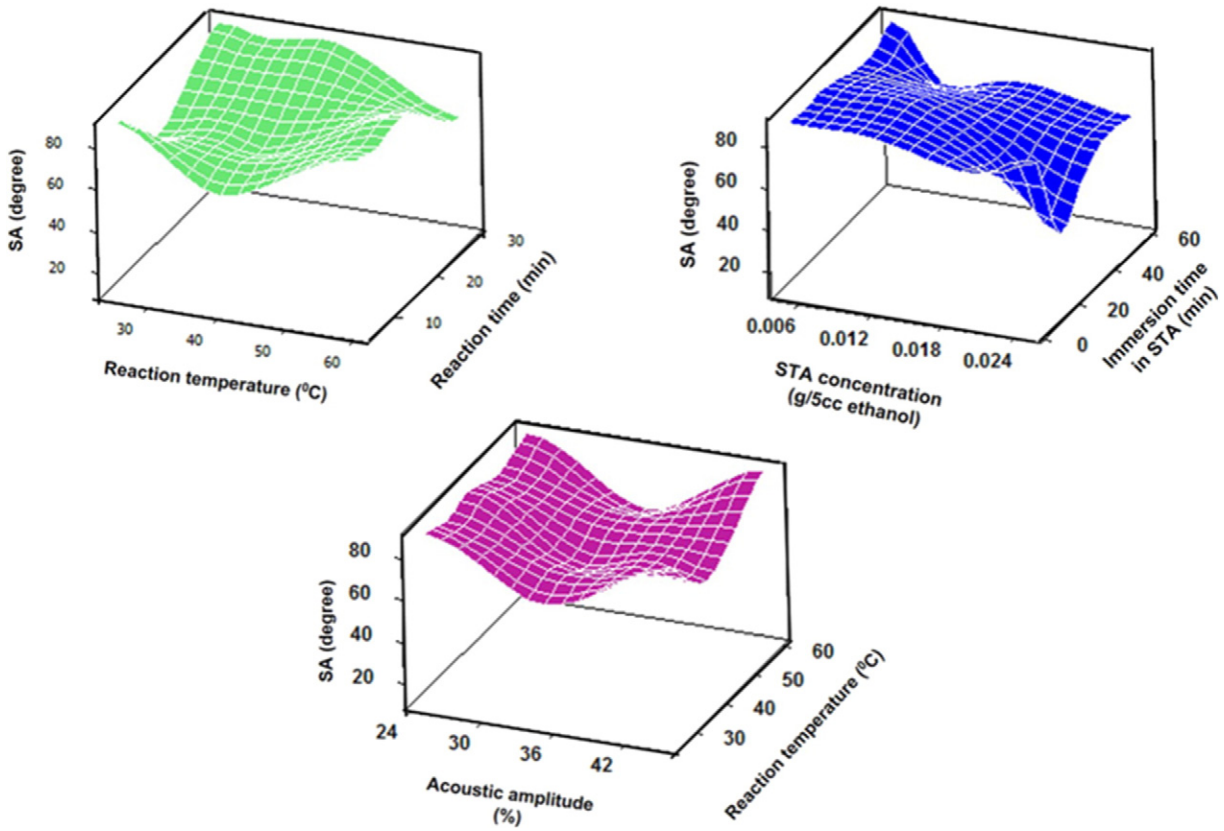

Fig. 2. Three-dimensional graphs of a) reaction time-reaction temperature-SA, b) STA concentration-immersion time in STA-SA and c) acoustic amplitude-reaction temperature-SA.

Table 3
The treatment conditions for both methods (ultrasound and the classical).

Method	Reaction time (min)	Reaction temperature (°C)	Acoustic amplitude (%)	STA concentration (g/5 cm^3 ethanol)	Immersion time in STA (min)	Starting material concentration (M)	Stirring rate (rpm)
Classical	15	40	–	0.025	60	0.01	500
Ultrasound	15	40	35	0.025	60	0.01	–

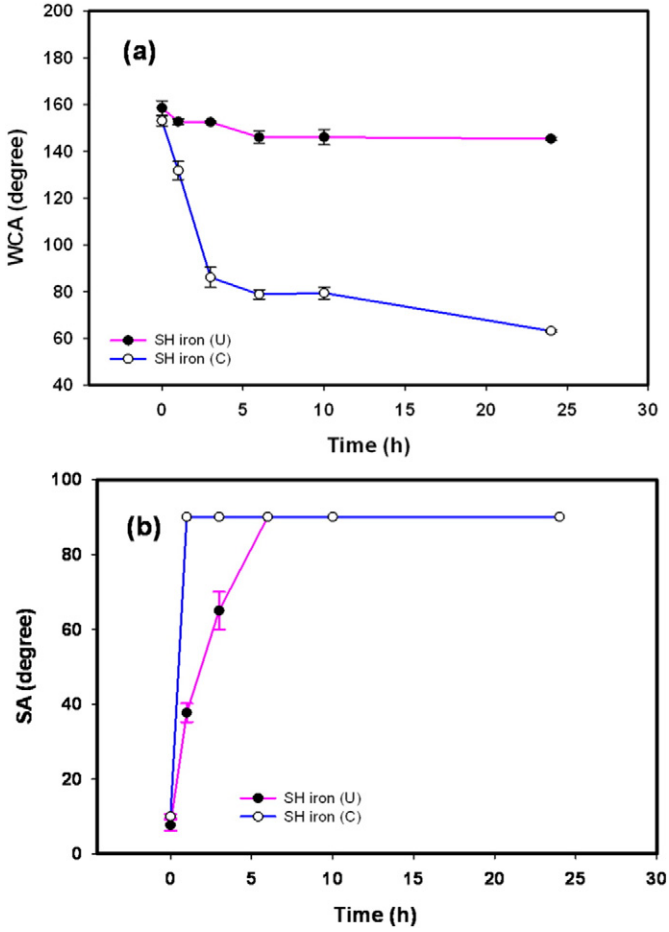

Fig. 4. a) WCA and b) SA values versus time immersion in NaCl solution (3.5%).

3.2. Data analysis

After carrying out all experiments, the results (SA values) were converted into RPD (relative percentage deviation) values according to the following formula.

$$RPD = |\text{Method sol-best sol}| \times 100/\text{best sol}$$

RPD is a dimensionless parameter. Method sol is SA value for each run of experiment and the best sol is the lowest value of SA in all 27-experiment runs. The RPD values are demonstrated in Table 1. The data analyzing are accomplished after RPD placing in response column. This analyzing will create two series of graphs named as mean of means and mean of SN (signal to noise) ratios (Fig. 1). We can confirm the optimized parameter values when the lowest point in mean of means graph was corresponded to the highest point in mean of SN graph. The lowest point in the mean of means graph assigns to the lowest RPD. If RPD values were smaller, it means that the deviation from best value is smaller at that point. So, for each parameter, the optimized value is the point that RPD has the lowest worth. Also, in this point with the lowest RPD, the SN ratios must be at the highest level. Based on this method, the optimized parameters are introduced in Table.2.

Three-dimensional diagrams are presented in Fig. 2. For each of represented graph, the effect of two variables is demonstrated on SA values. For example, in Fig. 2a, simultaneous effect of reaction time and reaction temperature is displayed on SA results. As it is clear from this figure, when reaction time and temperature are 15 min and 40 °C correspondingly, the lowest SA is obtained. Furthermore, based on Fig. 2b, it can be inferred that STA concentration of 0.025 g/5 cm^3 ethanol and 60 min immersion time in this solution will resulted in lowest SA. Finally, regarding the Fig. 2c, acoustic amplitude of 35% and reaction temperature of 40 °C are the best conditions to conclude SH iron surface with the lowest SA.

Therefore, five variables have been optimized based on Minitab software. However, the starting material concentration cannot be optimized using this method. Because, based on Fig. 1, the lowest RPD for starting material concentration is resulted for 0.01 M which is not corresponded to the highest point in mean of SN graph. As a result, for optimization of this factor, we must carry out a series of experiments at different concentrations of starting materials. It is worthy to emphasize that in all experiments the five other factors, which have been optimized previously, must be unchanged and fixed at their optimized levels. According to this illustration, the results are displayed in Fig. 3.

Undoubtedly, it can be inferred that when starting material concentration is 0.01 M, the high WCA and lowest SA has been acquired. Further concentration enhancement leads to WCA reduction to some extent. Consequently, starting material concentration of 0.01 M has been selected as optimized level. The SH iron surface, which is created

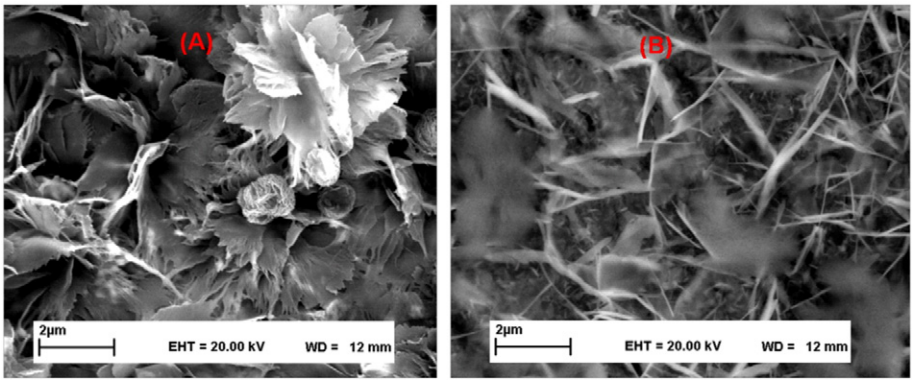

Fig. 5. SEM images of SH iron (U), A) before and B) after immersion in NaCl solution (3.5%) for 3 h.

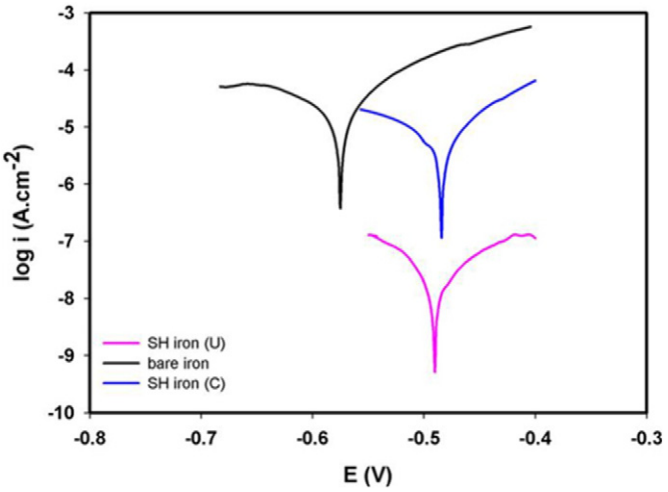

Fig. 6. Potentiodynamic polarization curves for bare iron, SH iron (U) and SH iron (C).

using optimized values of mentioned variables, demonstrates the high WCA (158.47° ± 3.14°) and lowest SA (7.66° ± 1.45°). The obtained surface has been named as SH iron (U) that U denotes to ultrasound approach. For having a comparison between ultrasound and classic methods, the SH iron has been fabricated based on simple immersion way without ultrasound. It must be noted that all variables have been selected at their optimized level, which were previously determined using Minitab software. Besides, for classic method, stirring was done instead of sonication. After ZnO deposition, surface energy reduction has been performed using STA solution (with concentration of 0.025 g/5 cm^3 ethanol and for 1 h immersion time). The results verify that classic method is able to produce SH iron (SH iron (C)). In this situation, WCA and SA values are 153.05° ± 2.12° and 10.00° ± 0.57°, respectively. So, both methods (classic and ultrasound) will result in SH iron. However, using corrosion resistance assessments, the sample prepared under ultrasound was more effective than the sample prepared in classical way. These results are demonstrated in the following section in details.

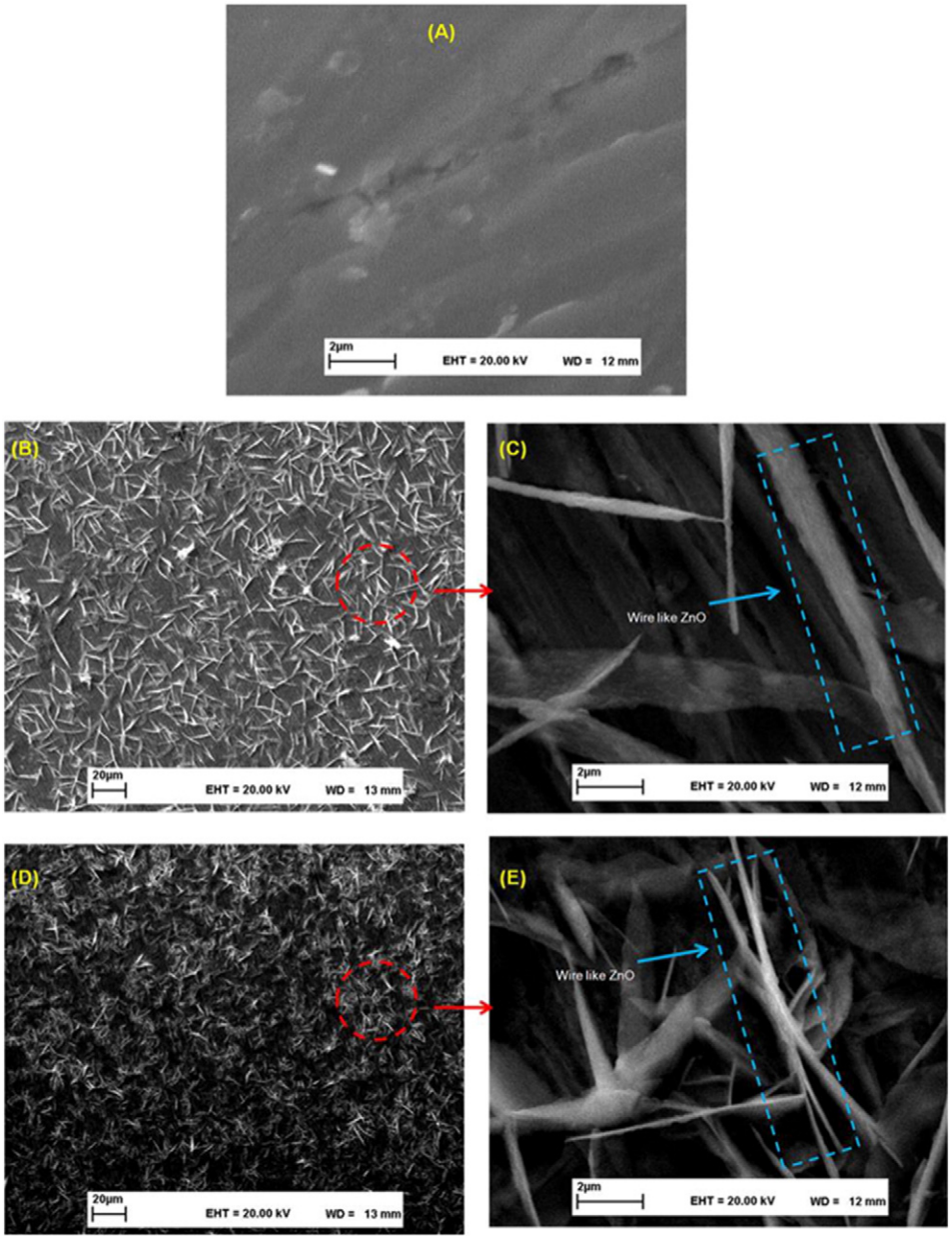

Fig. 7. SEM images of A) bare iron, B–C) ZnO-iron-C and D–E) ZnO-iron-U.

Table 3 shows the conditions which are adjusted to have SH iron via classical and ultrasound methods.

3.3. Corrosion resistance

For further study, the stability of SH iron using both classic and ultrasound methods in corrosive environment has been investigated. After immersion of SH iron (U) and SH iron (C) in NaCl solution (3.5%), the WCA determination has been conducted for various interval times. Based on Fig. 4a, it can be cited that after immersion of SH iron (C) in NaCl solution only for 1 h, the WCA value slumps and reaches to 131.78° ± 3.86° and further immersion up to 24 h, will conclude very low WCA of 63.12° ± 0.57°. Nevertheless, for SH iron (U) high WCA can be preserved for longer times. For this case, surface immersion in NaCl solution for 24 h will result in smaller reduction in WCA (145.28° ± 0.69°) compared to classic ones. Besides, the SA measurements were done at different interval times. As can be seen from Fig. 4 b, for SH iron (C) after immersion for 1 h, the SA value increased from 10.00° ± 0.57° to 90°. However, for SH iron (U) the SA increased from 7.66° ± 1.45° to 37.66° ± 2.51° for the same immersion time.

For observation of morphology changes after immersion in NaCl solution, the SEM image of SH iron (U) after 3 h immersion is shown in Fig. 5. According to Fig. 5A–B, the flower like structure on SH iron (U) destroys during this immersion time and indicates removal of STA from this surface.

In addition of immersion in NaCl solution, polarization curve measurement has been employed for the corrosion resistance examination. This measurement has been conducted based on Tafel extrapolation technique.

Two factors obtained from this method are corrosion current (I_c) and corrosion potential (E_c). When I_c demonstrates a fall trend and E_c shifts to positive direction, the corrosion resistance improvement can be concluded [24–27]. From Fig. 6, it can be pointed out that for bare iron E_c is −570 mV and this potential changes positively to −484 mV and −489 mV for SH iron (C) and SH iron (U), correspondingly. Moreover, I_c for bare iron is roughly 5.50×10^{-6} A·cm^{-2}. For SH iron (C), this current decreases threefold and reaches to about 1.77×10^{-6} A·cm^{-2}. Therefore, I_c reduction in this case is not notable. When ultrasound has been utilized as particle deposition method to obtain SH iron, the situation is different. In this case, I_c (8.72×10^{-3} A·cm^{-2}) is 1000 times lower than I_c of bare iron. Generally, for both SH surfaces (SH iron (U) and SH iron (C)), E_c transfers to positive direction and I_c drops off in comparison with bare iron. But, the reduction of I_c is more significant for SH iron (U). So, it can be inferred that for SH iron (U) surface, the improvement of corrosion resistance is more efficient in comparison with SH iron (C) ones.

In SH surfaces, there are huge fractions of entrapped air between the pits that reduce the contact region between solid surface and water. Consequently, SH surfaces can reject any kind of species with hydrophilic characteristic for example Cl^- ions with corrosive property. This rejection is a main reason for observation of the corrosion resistance improvement for SH surfaces. It is crucial to emphasize that more particle deposition can preserve more air pockets between the pits of surface as well as more stable SH surface will be concluded. Therefore, as ultrasound leads to more particle deposition on iron surface, the corrosion resistance elevates more too. For verification, it is essential to investigate SEM analysis that can demonstrate surface topography. It should be noted that, all characterizations have been carried out for surfaces at optimized condition of synthesis.

3.4. SEM and EDX analysis

According to Fig. 7, the SEM images of bare iron, ZnO-deposited iron with classic (ZnO-iron-C) and ultrasound (ZnO-iron-U) methods are represented. It is clear that, bare iron has a nearly smooth surface before any particle deposition (Fig. 7A). After ZnO particle deposition by means of classic approach (Fig. 7B, C), the presence of wire like structures is obvious on iron surface. These microstructures are appropriate places for air trapping. However, distribution of ZnO microstructures on the surface is not crowded and it is not in favor of SH state stability in NaCl solution. Ultrasound causes particle deposition with higher density (Fig. 7 D, E). This morphology provides suitable conditions for more air trapping as well as more hydrophilic species rejection from iron surface. Therefore, SH iron surface with enhanced stability is concluded for the

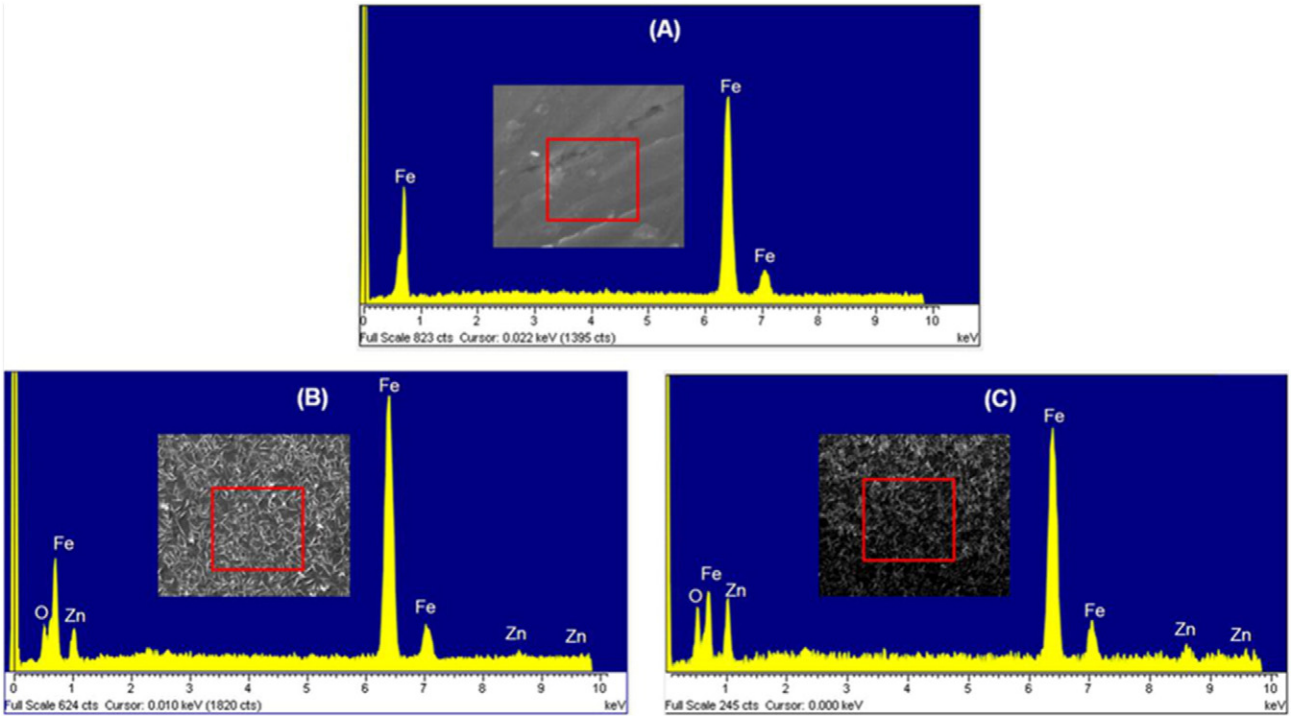

Fig. 8. EDX spectra of A) bare iron, B) ZnO-iron-C and C) ZnO-iron-U.

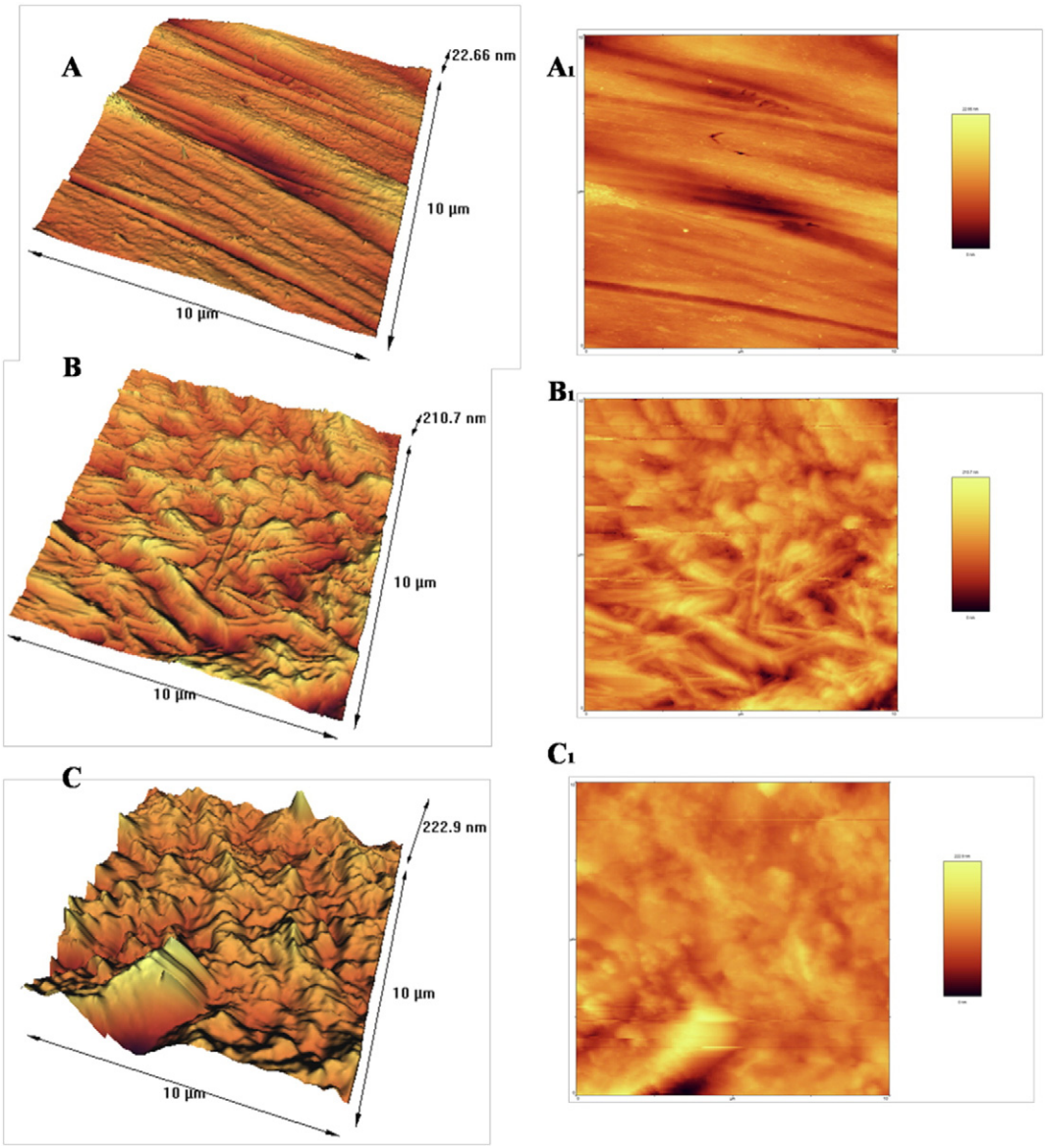

Fig. 9. 2D (right) and 3D (left) AFM images of (A, A_1) bare iron, (B, B_1) ZnO-iron-C and (C, C_1) ZnO-iron-U.

sample prepared under ultrasound. This durability was previously verified (Figs. 4 and 6). The distinctive conditions produced by ultrasound are major reason for different distribution of particles. Shock waves and microjets known as strong streams are created because of asymmetric collapse in heterogeneous medium. These streams lead to efficient collisions between particles. Consequently, further combination and agglomeration of particles can be observed on iron surface. In this situation, the entrapping of air pockets between surface pits will be increased which is the main reason for different behavior of SH iron (U) and SH iron (C) in corrosive environment.

Moreover, EDX analysis as a valuable method can reveal the presence of existing elements on iron surface. It is clear from Fig. 8A that, bare iron possess only Fe element. It means that there is not any additional element in iron surface. Furthermore, for ZnO-iron-C the

Table 4
Roughness parameters for bare iron, ZnO-iron-C and ZnO-iron-U surfaces.

Roughness parameter (nm)	Bare iron	ZnO-iron-C	ZnO-iron-U
R_a	0.121 ± 0.044	3.553 ± 0.597	3.767 ± 0.643
R_{ms}	1.172 ± 0.587	25.630 ± 3.301	23.008 ± 2.756

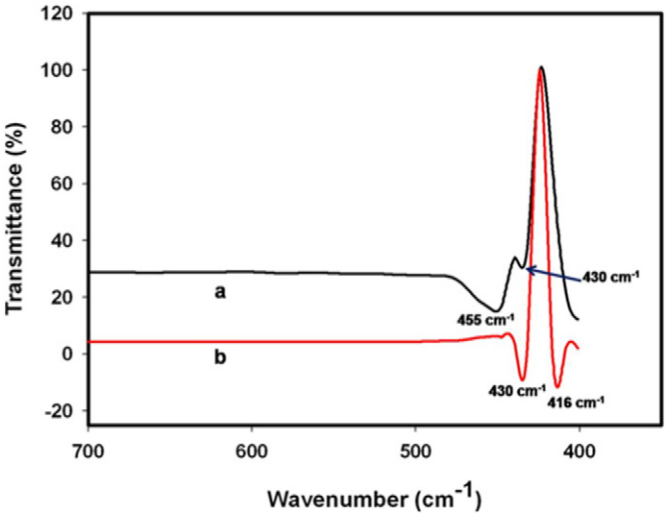

Fig. 10. ATR-FTIR spectra of a) bare iron and b) ZnO-iron-U surface.

appearance of Zn and O characteristic peaks can be an evidence for deposition of ZnO particles (Fig. 8B). Nevertheless, when ultrasound is employed for particle deposition, the Zn and O peaks become visible with enhanced intensity (Fig. 8C). Besides, the characteristic peak of Fe turns into weaker state. Therefore, EDX spectra prove more ZnO particle deposition on iron substrate using ultrasound instead of classic way. The acquired results are well matched with SEM outcomes.

3.5. AFM analysis

The images of AFM analysis are demonstrated in Fig. 9. Based on Fig. 9 A, A_1, the bare iron has nearly smooth surface. After ZnO deposition using classical (Fig. 9 B, B_1) and ultrasound (Fig. 9 C, C_1) methods, the roughness of surface increases dramatically, this is a sign of ZnO deposition on iron surface.

Moreover, the results of quantitative measurements of surface roughness, such as root mean square roughness (Rms) and mean roughness (Ra) are summarized in Table.4.

According to Table 4, it is obvious that roughness parameters change after ZnO deposition via classical and ultrasound methods and the roughness was improved by ZnO deposition. Finally, the thicknesses of deposited layers were estimated to roughly 70 nm based on AFM images for both methods.

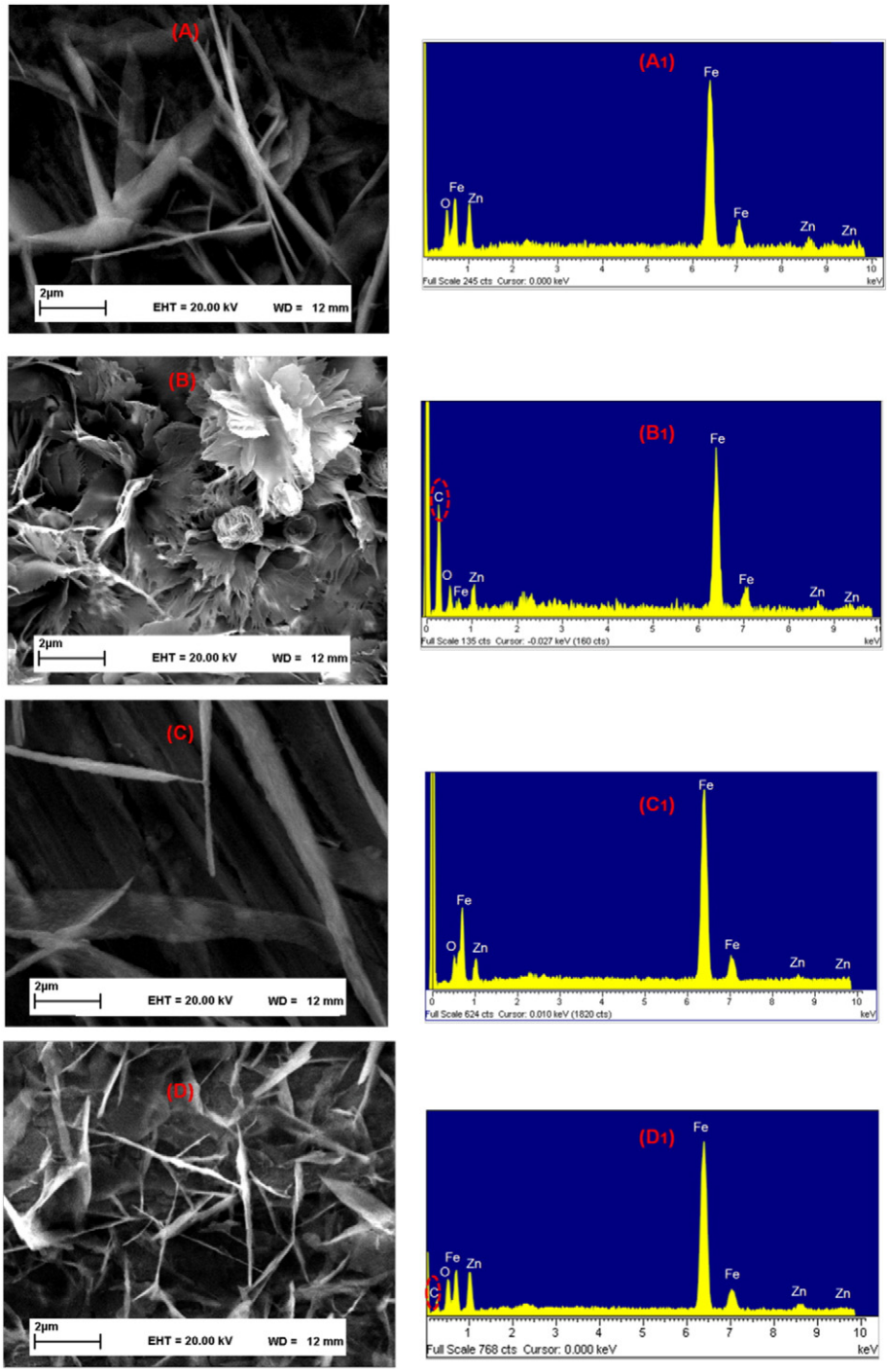

Fig. 11. SEM images (left) and EDX spectra (right) of (A, A_1) ZnO-iron-U, (B, B_1) SH iron (U), (C, C_1) ZnO-iron-C and (D, D_1) SH iron (C).

3.6. ATR-FTIR investigation

ATR-FTIR analysis is another method for verification of ZnO existence on iron surface. Based on Fig. 10, for bare iron there are two visible peaks at 433 cm^{-1} and 455 cm^{-1} that are related to Fe—O bonds vibration [17]. After deposition of ZnO particles using ultrasound, the emergence of characteristic peak of wurtzite ZnO is observable at 416 cm^{-1} [28]. Furthermore, after this deposition, the intensity of Fe—O characteristic peak (at 455 cm^{-1}) becomes weaker and can be a sign of ZnO particle deposition.

3.7. STA grafting verification

For creation of SH surface, the modification of ZnO-iron with STA is necessary. For STA grafting proof, EDX and SEM investigation has been carried out for SH iron (U) and SH iron (C) in comparison with respectively ZnO-iron-U and ZnO-iron-C. As it is obvious from Fig. 11, after STA modification in final step of SH surface creation, flower-like structure has been obtained on SH iron (U) (Fig. 11 B). These structures are because of STA-grafting. Besides, the emergence of strong new peak related to C element, can be a sign of STA presence on SH iron (Fig. 11 B_1). Also, for SH iron (C) the surface structure has been changed after STA grafting. But, compared to ultrasound method, the flower structure is not concluded and lower intensity of C element in EDX spectra (Fig. 11 D_1), can verify the lower STA presence of this surface.

4. Conclusion

In summary, SH surface creation was initially carried out using ZnO particle deposition. This deposition was done via both ultrasound and classic methods. For surface energy reduction STA ethanol solution was utilized. Minitab software was used for optimization of various parameters. SH iron with high WCA (158.47° ± 3.14°) and lowest SA (7.66° ± 1.45°) was achieved at predetermined optimized variables by Minitab software and named as SH iron (U). For comparison, particle deposition by the classic method was conducted based on simple immersion method. Using this approach SH iron with WCA of 153.05° ± 2.12° and SA of 10.00° ± 0.57° was resulted and known as SH iron (C). The SEM and EDX investigations exhibited further ZnO wire like distributions using ultrasound compared with the classical method. More particle deposition has significant influence on air trapping between surface grooves and as well as on enhancing the stability of acquired SH iron surface versus corrosive environment. The results show that for SH iron (U), I_c decreases significantly (1000 times lower than bare iron) in comparison with SH iron (C).

Acknowledgement

The support of Ferdowsi University of Mashhad, Iran (Research and Technology) for this work (code 3/29793, date 28/01/2014) is appreciated.

References

[1] R.-D.n.A. Sun, A.n.A. Nakajima, A.n.A. Fujishima, T.n.A. Watanabe, K. Hashimoto, Photoinduced Surface Wettability Conversion of ZnO and TiO^2 Thin FilmsDOI 2001.
[2] M. Miwa, A. Nakajima, A. Fujishima, K. Hashimoto, T. Watanabe, Effects of the surface roughness on sliding angles of water droplets on superhydrophobic surfaces, Langmuir 16 (2000) 5754–5760.
[3] A. Nakajima, A. Fujishima, K. Hashimoto, T. Watanabe, Preparation of transparent superhydrophobic boehmite and silica films by sublimation of aluminum acetylacetonate, Adv. Mater. 11 (1999) 1365–1368.
[4] L. Feng, S. Li, Y. Li, H. Li, L. Zhang, J. Zhai, Y. Song, B. Liu, L. Jiang, D. Zhu, Super-hydrophobic surfaces: from natural to artificial, Adv. Mater. 14 (2002) 1857–1860.
[5] J. Song, Y. Lu, S. Huang, X. Liu, L. Wu, W. Xu, A simple immersion approach for fabricating superhydrophobic Mg alloy surfaces, Appl. Surf. Sci. 266 (2013) 445–450.
[6] L.J. Chen, M. Chen, H. Di Zhou, J.M. Chen, Preparation of super-hydrophobic surface on stainless steel, Appl. Surf. Sci. 255 (2008) 3459–3462.
[7] M. Sun, C. Luo, L. Xu, H. Ji, Q. Ouyang, D. Yu, Y. Chen, Artificial lotus leaf by nanocasting, Langmuir 21 (2005) 8978–8981.
[8] M.R. Cardoso, V. Tribuzi, D.T. Balogh, L. Misoguti, C.R. Mendonça, Laser microstructuring for fabricating superhydrophobic polymeric surfaces, Appl. Surf. Sci. 257 (2011) 3281–3284.
[9] C. Dong, Y. Gu, M. Zhong, L. Li, K. Sezer, M. Ma, W. Liu, Fabrication of superhydrophobic Cu surfaces with tunable regular micro and random nano-scale structures by hybrid laser texture and chemical etching, J. Mater. Process. Technol. 211 (2011) 1234–1240.
[10] J.P. Fernández-Blázquez, D. Fell, E. Bonaccurso, A.d. Campo, Superhydrophilic and superhydrophobic nanostructured surfaces via plasma treatment, J. Colloid Interface Sci. 357 (2011) 234–238.
[11] Z. Yuan, H. Chen, J. Zhang, Facile method to prepare lotus-leaf-like super-hydrophobic poly(vinyl chloride) film, Appl. Surf. Sci. 254 (2008) 1593–1598.
[12] Z. Meng, Q. Wang, X. Qu, C. Zhang, J. Li, J. Liu, Z. Yang, Papillae mimetic hairy composite spheres towards lotus leaf effect coatings, Polymer 52 (2011) 597–601.
[13] W. Liu, Y. Luo, L. Sun, R. Wu, H. Jiang, Y. Liu, Fabrication of the superhydrophobic surface on aluminum alloy by anodizing and polymeric coating, Appl. Surf. Sci. 264 (2013) 872–878.
[14] Y. Wei, R. Adamson, J. Dempsey, Ice/metal interfaces: fracture energy and fractography, J. Mater. Sci. 31 (1996) 943–947.
[15] M. Liang, Y. Wei, L. Hou, H. Wang, Y. Li, C. Guo, Fabrication of a super-hydrophobic surface on a magnesium alloy by a simple method, J. Alloys Compd. 656 (2016) 311–317.
[16] D. Zang, R. Zhu, C. Wu, X. Yu, Y. Zhang, Fabrication of stable superhydrophobic surface with improved anticorrosion property on magnesium alloy, Scr. Mater. 69 (2013) 614–617.
[17] K. Li, X. Zeng, H. Li, X. Lai, A study on the fabrication of superhydrophobic iron surfaces by chemical etching and galvanic replacement methods and their anti-icing properties, Appl. Surf. Sci. 346 (2015) 458–463.
[18] H.-J. Song, X.-Q. Shen, H.-Y. Ji, X.-J. Jing, Superhydrophobic iron material surface with flower-like structures obtained by a facile self-assembled monolayer, Appl. Phys. A Mater. Sci. Process. 99 (2010) 685–689.
[19] N. Wang, D. Xiong, Y. Deng, Y. Shi, K. Wang, Mechanically robust superhydrophobic steel surface with anti-icing, UV-durability, and corrosion resistance properties, ACS Appl. Mater. Interfaces 7 (2015) 6260–6272.
[20] Z. Sharifalhoseini, M.H. Entezari, R. Jalal, Direct and indirect sonication affect differently the microstructure and the morphology of ZnO nanoparticles: optical behavior and its antibacterial activity, Ultrason. Sonochem. 27 (2015) 466–473.
[21] V. Romero, I. Costas-Mora, I. Lavilla, C. Bendicho, In situ ultrasound-assisted synthesis of Fe 3 O 4 nanoparticles with simultaneous ion co-precipitation for multielemental analysis of natural waters by total reflection X-ray fluorescence spectrometry, J. Anal. At. Spectrom. 28 (2013) 923–933.
[22] K. Okitsu, M. Ashokkumar, F. Grieser, Sonochemical synthesis of gold nanoparticles: effects of ultrasound frequency, J. Phys. Chem. B 109 (2005) 20673–20675.
[23] I.A. Wani, A. Ganguly, J. Ahmed, T. Ahmad, Silver nanoparticles: ultrasonic wave assisted synthesis, optical characterization and surface area studies, Mater. Lett. 65 (2011) 520–522.
[24] D. Lv, J. Ou, M. Xue, F. Wang, Stability and corrosion resistance of superhydrophobic surface on oxidized aluminum in NaCl aqueous solution, Appl. Surf. Sci. 333 (2015) 163–169.
[25] S. Khorsand, K. Raeissi, F. Ashrafizadeh, Corrosion resistance and long-term durability of super-hydrophobic nickel film prepared by electrodeposition process, Appl. Surf. Sci. 305 (2014) 498–505.
[26] L. Feng, H. Zhang, Z. Wang, Y. Liu, Superhydrophobic aluminum alloy surface: fabrication, structure, and corrosion resistance, Colloids Surf. A Physicochem. Eng. Asp. 441 (2014) 319–325.
[27] T. Rezayi, M.H. Entezari, Towards a durable superhydrophobic aluminum surface by etching and ZnO nanoparticle deposition, J. Colloid Interface Sci. 463 (2016) 37–45.
[28] T. Ivanova, A. Harizanova, T. Koutzarova, B. Vertruyen, Preparation and characterization of ZnO–TiO 2 films obtained by sol-gel method, J. Non-Cryst. Solids 357 (2011) 2840–2845.